5352 J. Med. Chem. 2010, 53, 5352–5355
DOI: 10.1021/jm100249w

Journal of Medicinal Chemistry
Brief Article

Structural Basis for the Interaction between Tankyrase-2 and a Potent Wnt-Signaling Inhibitor†

Tobias Karlberg,‡ Natalia Markova,‡,§ Ida Johansson,‡ Martin Hammarström,‡ Patrick Schütz,‡ Johan Weigelt,‡ and Herwig Schüler*,‡

‡Structural Genomics Consortium, Department of Medical Biochemistry and Biophysics, Karolinska Institutet, S-17177 Stockholm, Sweden, and §iNovacia AB, S-11251 Stockholm, Sweden

Received February 24, 2010

We report two crystal structures of the PARP domain of human tankyrase-2 (TNKS2). Tankyrases are involved in fundamental cellular processes such as telomere homeostasis and Wnt signaling. The complex of TNKS2 with the potent inhibitor XAV939 provides insights into the molecular basis of the strong interaction and suggests routes for further development of tankyrase inhibitors.

Introduction

Tankyrases (TNKS1 and TNKS2) belong to the poly ADP-ribose polymerases (PARP[a]) family of proteins, comprising 17 proteins that all share a catalytic PARP domain.[1,2] PARP proteins act by mono- or poly-ADP-ribosylation of target proteins to confer cellular signals (Supporting Information Figure S1). PARP1 and PARP2, the most well-characterized family members, are key components in homologous recombination DNA damage response. They have been pursued as cancer drug targets for more than a decade,[3] and PARP1/2 inhibitors have shown promising results in clinical trials.[4,5] Cellular functions of many of the other PARP proteins remain to be identified.

Recently the tankyrases have gained increased attention as potential drug targets. Tankyrases are positive regulators of telomere elongation; they poly-ADP-ribosylate Telomeric repeat-binding factor 1 (TRF1), thereby causing disruption of the protein complex that protects telomeres, resulting in telomerase access to telomere ends.[6,7] Tankyrases also mark the β-catenin destruction complex component axin for degradation, and tankyrase inhibition antagonizes the Wnt signal transduction pathway by stimulating β-catenin degradation.[8] Moreover, tankyrase inhibition imposes selective lethality on BRCA deficient cell lines.[9] Thus, inhibition of tankyrase activity is appearing as a promising strategy for targeting cancer by diverse mechanisms. The two highly homologous tankyrase isoforms in human, TNKS1/PARP5a/ARTD5[7] and TNKS2/PARP5b/ARTD6,[10,11] share PARP catalytic domains (TNKS1$^{1091-1313}$ and TNKS2$^{938-1160}$) that are 86% identical and 95% similar. The residues lining the active site show a high degree of conservation among all PARP family members. Detailed insights into the structural basis of ligand recognition, as well as characterization of inhibitor crossreactivity, are therefore important to understand and potentially minimize off-target effects. Moreover, isoform selective inhibitors will be key to elucidating the biological functions of individual PARPs.

In this study we report the first high resolution structure of a tankyrase in complex with an inhibitor and describe the structural basis for its selectivity for tankyrases over PARP1 and PARP2.

Results

2-(4-(Trifluoromethyl)phenyl)-7,8-dihydro-5*H*-thiopyrano-[4,3-*d*]pyrimidin-4-ol (XAV939, **1**, Figure 1a) was recently identified as the first high potency inhibitor of TNKS1 and TNKS2, with 10- to 500-fold selectivity for the tankyrases over PARP1 and -2.[8] We soaked **1** into crystals of the TNKS2 PARP-domain (residues 946−1162 supplemented with an N-terminal hexahistidine tag) that had been obtained by an in situ proteolysis crystallization strategy[12] and determined the structures of TNKS2 bound to **1** and ligand-free TNKS2 to atomic resolution (see Supporting Information for details). The apo and inhibitor bound structures are highly similar, with a backbone rmsd of 0.3 Å. The inhibitor complex reveals that **1** is anchored in the nicotinamide crevice of the NAD^+ binding site by similar interactions as observed for other PARP inhibitor complexes.[13,14] The Tyr1071 side chain stacks with the pyrimidine ring, and the Ser1068 hydroxyl and the Gly1032 backbone oxygen and nitrogen hydrogen bond stack with the pyrimidine nitrogen and pyrimidinol hydroxyl (Figure 1b and Figure 1c). The sulfur atom in the thiopyrano ring is within hydrogen bonding distance of the Phe1061 backbone. The remaining interactions between **1** and the protein have nonpolar character: The phenyl ring resides in a cleft lined by the Tyr1050 and Tyr1071 side chains, and the distal trifluoromethyl group of **1** makes nonpolar contacts with the Pro1034, Phe1035, and Ile1075 side chains. Surface rendering of the protein illustrates the tight fit of **1** in the NAD^+ binding pocket (Figure 1b). The in situ proteolysis caused a nick in the loop between strands 6 and 7 (dotted line in Figure 1d). This cleaved loop is located on the surface of the protein at ~10 Å distance from the active site. In TNKS1 the corresponding loop between strands 6 and 7 could be modeled into the electron density and is involved in crystal packing. Importantly, neither the active site nor the overall structure of TNKS2 is affected by loop cleavage, as demonstrated by the ability of cleaved TNKS2 to bind inhibitor and by the good

†PDB codes for the TNKS2 structures are 3KR7 and 3KR8.

*To whom correspondence should be addressed. Phone: +46852486843. Fax: +46852486868. E-mail: herwig.schuler@ki.se.

[a] Abbreviations: ITC, isothermal titration calorimetry; NAD^+, nicotinamide adenine dinucleotide; PARP, poly ADP-ribose polymerase.

 Published on Web 06/21/2010

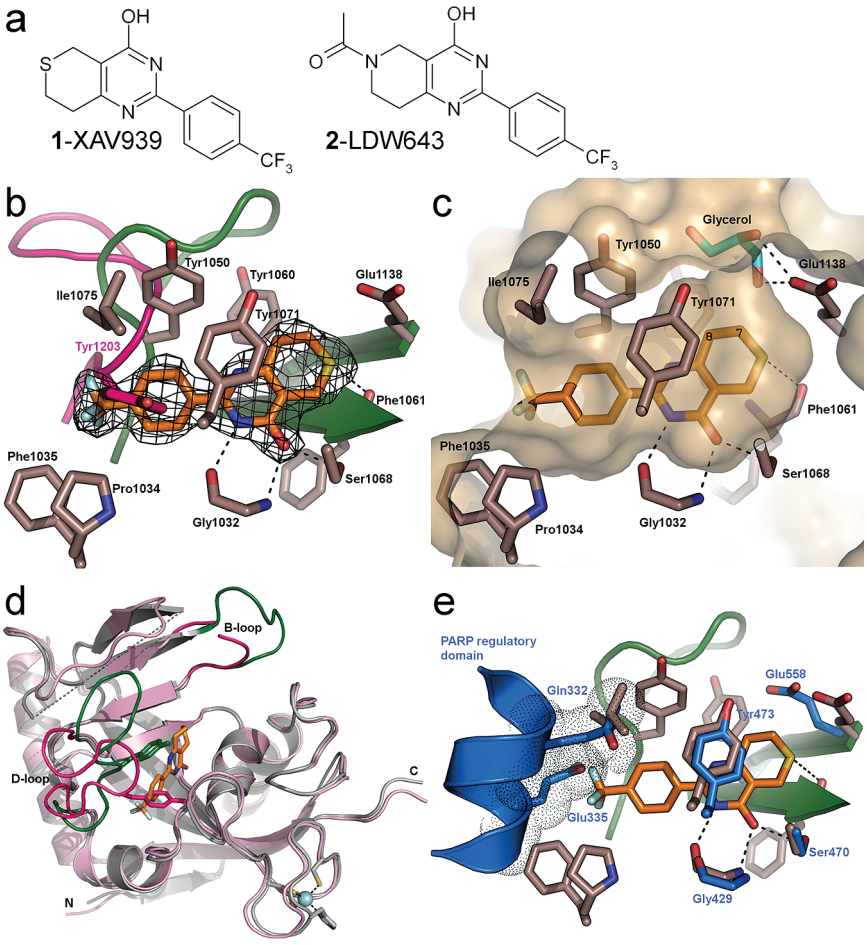

Figure 1. (a) Molecular structures of **1** and **2**. (b−e) Structure of the PARP domain of TNKS2 in complex with inhibitor **1**. (b) Compound **1** binding site and interactions between compound and protein. Electron density ($2F_{obs} - F_{calc}$) rendered at 1.5σ is shown for the inhibitor. The D-loop of the superimposed TNKS1 apo structure is shown in pink. (c) Surface representation of the protein, illustrating the fit of **1** in the NAD^+ pocket. (d) Superposition of TNKS1 and TNKS2, colored as in (b). (e) PARP2 (in blue; PDB entry 3KJD) superimposed onto the **1**-occupied ligand binding pocket of TNKS2, illustrating the positioning of α-helix-5 of the regulatory domain near the NAD^+ cleft opening, and conserved side chains in the nicotinamide binding crevice.

superimposition with the TNKS1 structure (backbone rmsd of 0.9 Å over 155 residues) (Figure 1d).

Discussion and Conclusions

The study by Huang et al. revealed tight binding of **1** to both tankyrases with a slight preference for TNKS2 over TNKS1 (IC_{50} of 4 and 11 nM), which was corroborated by binding of Cy5-labeled **1** to TNKS2 and TNKS 1 (K_d of 10 and 100 nM).[8] We confirmed the high potency of **1** using isothermal titration calorimetry (ITC) and determined K_d values of 8 nM for the interaction with TNKS2 and 14 nM with TNKS1 fitting to a 1:1 binding model (Figure 2 and Table 1). Superposition of the TNKS2 structures with the TNKS1 apo structure[15] reveals different conformations of the donor site loop (D-loop) (Figure 1b and Figure 1d). Assuming similar binding modes of **1** in both tankyrases, the D-loop conformation in the TNKS1 apo structure is incompatible with binding of **1**: Compound **1** would clash with the TNKS1-Tyr1203 side chain, whereas the corresponding TNKS2-Tyr1050 is within van der Waals distance of the phenyl moiety of the inhibitor (Figure 1b and Figure 1d). Since **1** binds TNKS1 with high affinity (Figure 2 and ref 8), the D-loop must be flexible in order to accommodate the inhibitor.

Binding of **1** to the tankyrases is enthalpically and entropically favorable, with a slightly stronger enthalpic contribution to TNKS2 binding (Table 1). In the absence of a TNKS1−**1** complex structure it is impossible to suggest a structural basis for the small selectivity for TNKS2 over TNKS1. The active sites are highly conserved, and the D-loop of TNKS1 is expected to adopt a similar conformation as in TNKS2 upon inhibitor binding. More importantly **1** displays a pronounced selectivity for the tankyrases over PARP1 (K_d = 0.62 μM for PARP1; Figure 2 and Table 1). This corroborates the ~200-fold selectivity over PARP1 and PARP2 observed in biochemical experiments reported by Huang et al.[8] Our structures provide a basis for interpreting this finding. First, the steric fit of **1** in the active site of TNKS2 is excellent (Figure 1b). Second, **1** is anchored by the conserved polar interactions discussed above, but most of interactions with the protein are nonpolar. By contrast, the NAD^+ binding pockets of other PARPs are lined by more polar side chains, and polar contacts dominate their interactions with inhibitors.[13,14,16] Finally, the trifluoromethyl group of the inhibitor makes nonpolar contacts with TNKS2 side chains near the pocket opening, as described (Figure 1a). Superpositions suggest similar interactions in the TNKS1−**1** complex. For PARP1 and -2, by contrast, the trifluoromethyl group would sterically clash with the regulatory domain, which would have to move slightly to accommodate **1** in the conformation observed in the TNKS2 complex (Figure 1e).

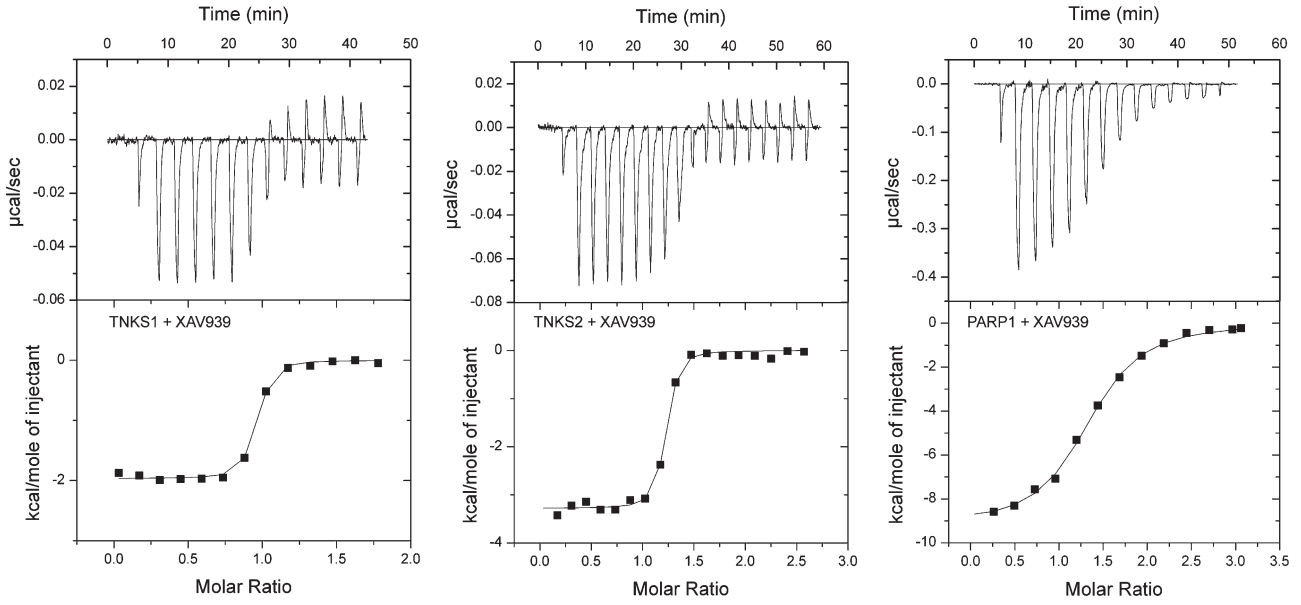

Figure 2. Isothermal titration calorimetry of TNKS1, TNKS2, and PARP1 with **1**. Titration raw data are shown in the upper plots, and integrated heat measurements are in the lower plots. Representative results and full data, including K_d values derived from all experiments, are reported in Table 1.

Table 1. Calorimetric Properties of Compound **1** Binding to TNKS1, TNKS2, and PARP1[a]

	K_d, nM	N	ΔH, kcal/mol	ΔS, cal/mol
TNKS1	14 ± 8	0.92 ± 0.01	−2.4 ± 0.4	28 ± 3
TNKS2	8 ± 3	1.09 ± 0.08	−3.7 ± 0.4	25 ± 1
PARP1	620 ± 130	1.35 ± 0.09	−9.3 ± 0.1	2.6 ± 0.5

[a] All values are reported as the mean ± SD based on three experiments. K_d values were obtained by fitting to a standard one-site binding model.

The TNKS2−**1** complex crystal structure suggests routes to optimize tankyrase inhibitors based on the **1** scaffold: (i) 1-(4-hydroxy-2-(4-(trifluoromethyl)phenyl)-7,8-dihydropyrido-[4,3-*d*]pyrimidin-6(5*H*)-yl)ethanone (LDW643, **2**, Figure 1a) is a close analogue of **1** that does not inhibit tankyrases.[8] Superimposing **2** onto **1** in our crystal structure suggests a steric clash between the acyl moiety of **2** and Phe1061-Ala1062. We conclude that addition of a bulky substituent at the position corresponding to the sulfur of the thiopyrano ring is incompatible with binding to tankyrases. (ii) Substitutions at the location of the trifluoromethyl group could establish additional interactions, e.g., with the Ala1049 carbonyl near the opening of the binding crevice (Figure 1b and Supporting Information Figure S1). (iii) The structure reveals a glycerol moiety bound in the vicinity of the thiopyrano ring of the inhibitor (Supporting Information Figure S1). This space is likely chemically accessible by substitutions at the 7 and 8 positions of the thiopyrano moiety to establish polar interactions with, for example, the catalytic glutamate (Glu1138). In summary, the present structures provide insights into the structural basis for **1** interactions with tankyrases, which will be important for further optimization of PARP inhibitors in general and tankyrase inhibitors in particular.

Experimental Section

Detailed experimental procedures are given in the Supporting Information. Briefly, all proteins were produced in *Escherichia coli* and purified using Ni^{2+}-chelating chromatography as previously described.[13] Crystals of chymotrypsin treated TNKS2$^{946-1162}$ were obtained in sitting drops at 4 °C in 0.1 M Tris-HCl, pH 8.5, 15−20% PEG3350, and 0.2 M lithium sulfate. Diffraction data for ligand-free TNKS2 were collected at the Diamond synchrotron radiation light source, beamline I03 (Oxfordshire, U.K.). The structure was solved by molecular replacement using PDB entry 2rf5 as template. Crystal complexes with **1** were obtained by incubating **1** with preformed crystals for 10 days at 4 °C. Diffraction data for complex crystals were collected with Cu Kα radiation on an X8 PROTEUM system (Bruker AXS). The structure was solved by molecular replacement with the apo structure as template. Details on data processing and refinement statistics are given in the Supporting Information Table S1. Isothermal titration calorimetry was performed at 25 °C with protein solutions at 5−10 μM in 20 mM HEPES, pH 7.5, 300 mM NaCl, 2 mM TCEP using a VP-ITC calorimeter (MicroCal, GE Healthcare Life Sciences).

Acknowledgment. We thank the beamline staff at the Diamond synchrotron radiation light source (Oxfordshire, U.K.) for expert assistance during data collection and Anna-Lena Gustavsson for helpful discussions. The Structural Genomics Consortium is a registered charity (No. 1097737) that receives funds from the Canadian Institutes for Health Research; the Canada Foundation for Innovation; Genome Canada through the Ontario Genomics Institute; GlaxoSmithKline; Karolinska Institutet; the Knut and AliceWallenberg Foundation; the Ontario Innovation Trust; the Ontario Ministry for Research and Innovation; Merck & Co., Inc.; the Novartis Research Foundation; the Swedish Agency for Innovation Systems; the Swedish Foundation for Strategic Research; and the Wellcome Trust.

Supporting Information Available: Table summarizing data collection and refinement statistics; figures summarizing PARP enzymatic action and illustrating details of the **1**−TNKS2 interaction; Materials and Methods section. This material is available free of charge via the Internet at http://pubs.acs.org.

References

(1) Amé, J. C.; Spenlehauer, C.; de Murcia, G. The PARP superfamily. *BioEssays* **2004**, *26*, 882–893.
(2) Hottiger, M. O.; Hassa, P. O.; Lüscher, B.; Schüler, H.; Koch-Nolte, F. Toward a unified nomenclature for mammalian ADP-ribosyltransferases. *Trends Biochem. Sci.* **2010**, *35*, 208–219.

(3) Martin, S. A.; Lord, C. J.; Ashworth, A. DNA repair deficiency as a therapeutic target in cancer. *Curr. Opin. Genet. Dev.* **2008**, *18*, 80–86.
(4) Fong, P. C.; Boss, D. S.; Yap, T. A.; Tutt, A.; Wu, P.; Mergui-Roelvink, M.; Mortimer, P.; Swaisland, H.; Lau, A.; O'Connor, M. J.; Ashworth, A.; Carmichael, J.; Kaye, S. B.; Schellens, J. H.; de Bono, J. S. Inhibition of poly(ADP-ribose) polymerase in tumors from BRCA mutation carriers. *N. Engl. J. Med.* **2009**, *361*, 123–134.
(5) Rouleau, M.; Patel, A.; Hendzel, M. J.; Kaufmann, S. H.; Poirier, G. G. PARP inhibition: PARP1 and beyond. *Nat. Rev. Cancer* **2010**, *10*, 293–301.
(6) Smith, S.; de Lange, T. Tankyrase promotes telomere elongation in human cells. *Curr. Biol.* **2000**, *10*, 1299–1302.
(7) Smith, S.; Giriat, I.; Schmitt, A.; de Lange, T. Tankyrase, a poly(ADP-ribose) polymerase at human telomeres. *Science* **1998**, *282*, 1484–1487.
(8) Huang, S. M.; Mishina, Y. M.; Liu, S.; Cheung, A.; Stegmeier, F.; Michaud, G. A.; Charlat, O.; Wiellette, E.; Zhang, Y.; Wiessner, S.; Hild, M.; Shi, X.; Wilson, C. J.; Mickanin, C.; Myer, V.; Fazal, A.; Tomlinson, R.; Serluca, F.; Shao, W.; Cheng, H.; Shultz, M.; Rau, C.; Schirle, M.; Schlegl, J.; Ghidelli, S.; Fawell, S.; Lu, C.; Curtis, D.; Kirschner, M. W.; Lengauer, C.; Finan, P. M.; Tallarico, J. A.; Bouwmeester, T.; Porter, J. A.; Bauer, A.; Cong, F. Tankyrase inhibition stabilizes axin and antagonizes Wnt signalling. *Nature* **2009**, *461*, 614–620.
(9) McCabe, N.; Cerone, M. A.; Ohishi, T.; Seimiya, H.; Lord, C. J.; Ashworth, A. Targeting tankyrase 1 as a therapeutic strategy for BRCA-associated cancer. *Oncogene* **2009**, *28*, 1465–1470.
(10) Amé, J. C.; Rolli, V.; Schreiber, V.; Niedergang, C.; Apiou, F.; Decker, P.; Muller, S.; Höger, T.; Ménissier-de Murcia, J.; de Murcia, G. PARP-2, a novel mammalian DNA damage-dependent poly(ADP-ribose) polymerase. *J. Biol. Chem.* **1999**, *274*, 17860–17868.
(11) Kaminker, P. G.; Kim, S. H.; Taylor, R. D.; Zebarjadian, Y.; Funk, W. D.; Morin, G. B.; Yaswen, P.; Campisi, J. TANK2, a new TRF1-associated poly(ADP-ribose) polymerase, causes rapid induction of cell death upon overexpression. *J. Biol. Chem.* **2001**, *276*, 35891–35899.
(12) Wernimont, A.; Edwards, A. In situ proteolysis to generate crystals for structure determination: an update. *PLoS One* **2009**, *4*, e5094.
(13) Lehtiö, L.; Jemth, A. S.; Collins, R.; Loseva, O.; Johansson, A.; Markova, N.; Hammarström, M.; Flores, A.; Holmberg-Schiavone, L.; Weigelt, J.; Helleday, T.; Schüler, H.; Karlberg, T. Structural basis for inhibitor specificity in human poly(ADP-ribose) polymerase-3. *J. Med. Chem.* **2009**, *52*, 3108–3111.
(14) Ruf, A.; de Murcia, G.; Schulz, G. E. Inhibitor and NAD+ binding to poly(ADP-ribose) polymerase as derived from crystal structures and homology modeling. *Biochemistry* **1998**, *37*, 3893–3900.
(15) Lehtiö, L.; Collins, R.; van den Berg, S.; Johansson, A.; Dahlgren, L. G.; Hammarström, M.; Helleday, T.; Holmberg-Schiavone, L.; Karlberg, T.; Weigelt, J. Zinc binding catalytic domain of human tankyrase 1. *J. Mol. Biol.* **2008**, *379*, 136–145.
(16) Karlberg, T.; Hammarström, M.; Schütz, P.; Svensson, L.; Schüler, H. Crystal structure of the catalytic domain of human PARP2 in complex with PARP inhibitor ABT-888. *Biochemistry* **2010**, *49*, 1056–1058.